Hindawi Publishing Corporation
Journal of Chemistry
Volume 2013, Article ID 945348, 6 pages
http://dx.doi.org/10.1155/2013/945348

Research Article

Mesoporous Metal-Containing Carbon Nitrides for Improved Photocatalytic Activities

Jie Luo,[1] Zhao-Jie Cui,[1] and Guo-Long Zang[2]

[1] *School of Environmental Science and Engineering, Shandong University, Jinan 250100, China*
[2] *Tianjin Renewable Resources Institute, All China Federation of Supply and Marketing Cooperatives, Tianjin 300191, China*

Correspondence should be addressed to Zhao-Jie Cui; cuizj@sdu.edu.cn and Guo-Long Zang; guolongz@gmail.com

Received 30 September 2013; Accepted 14 October 2013

Academic Editor: Tifeng Jiao

Graphitic carbon nitrides (g-C_3N_4) have attracted increasing interest due to their unusual properties and promising applications in water splitting, heterogeneous catalysis, and organic contaminant degradation. In this study, a new method was developed for the synthesis of mesoporous Fe contained g-C_3N_4 (m-Fe-C_3N_4) photocatalyst by using SiO_2 nanoparticles as hard template and dicyandiamide as precursor. The physicochemical properties of m-Fe-C_3N_4 were thoroughly investigated. The XRD and XPS results indicated that Fe was strongly coordinated with the g-C_3N_4 matrix and that the doping and mesoporous structure partially deteriorated its crystalline structure. The UV-visible absorption spectra revealed that m-Fe-C_3N_4 with a unique electronic structure displays an increased band gap in combination with a slightly reduced absorbance, implying that mesoporous structure modified the electronic properties of g-Fe-C_3N_4. The photocatalytic activity of m-Fe-C_3N_4 for photodegradation of Rhodamine B (RhB) was much higher than that of g-Fe-C_3N_4, clearly demonstrating porous structure positive effect.

1. Introduction

Carbon nitride has been widely regarded as the most promising candidate to complement carbon in materials applications. Among various carbon nitride compounds, graphitic carbon nitride (g-C_3N_4) is the most stable allotrope, which has attracted much attention for its potential application in splitting water, decomposing organic pollutants, and photosynthesis under visible light [1–5]. The polymeric g-C_3N_4 material contains graphitic stacking of C_3N_4 layers, which are constructed from tri-s-triazine units connected by planar amino groups [2, 6]. To further improve the performance of g-C_3N_4, many methods such as introducing functional atoms (B, F, S, P, etc.), controlling shape, and oxidation reaction have been used for its modification [1, 7–10].

One important way to improve its light utilization efficiency is to reduce the band gap and extend the light absorption range. Metal element dopants are usually introduced to prepare functional organic-metal hybrid material based on g-C_3N_4. Wang et al. firstly reported the synthesis of metal (Fe^{3+})-containing carbon nitride compounds using dicyandiamide and metal chloride as precursors, and such synthesized carbon nitride showed high photocatalytic activities for the degradation of various organic dyes [11]. g-C_3N_4 photocatalyst was also modified with other transition metal elements (Co, Ni, Mn, Cu [12], or Zn [13]) to obtain the high photocatalytic activity and good stability. It also was active for the direct oxidation of benzene to phenol using hydrogen peroxide [14].

The porous structure can increase the semiconductor surface area, which contributes to an enhancement in energy conversion efficiency [15, 16]. Herein, we report the synthesis of porous m-Fe-C_3N_4 photocatalysts by using SiO_2 nanoparticles as template and dicyandiamide as precursor, and the physicochemical properties of synthesized m-Fe-C_3N_4 and g-Fe-C_3N_4 were characterized by X-ray diffractometer (XRD), transmission electron microscopy (TEM), UV-visible spectrophotometer (UV-vis), X-ray photoelectron spectroscopy (XPS), Fourier transform infrared (FTIR) spectra, and N_2 adsorption-desorption measurement. Moreover, their performance for photodegradation of Rhodamine B (RhB) was evaluated.

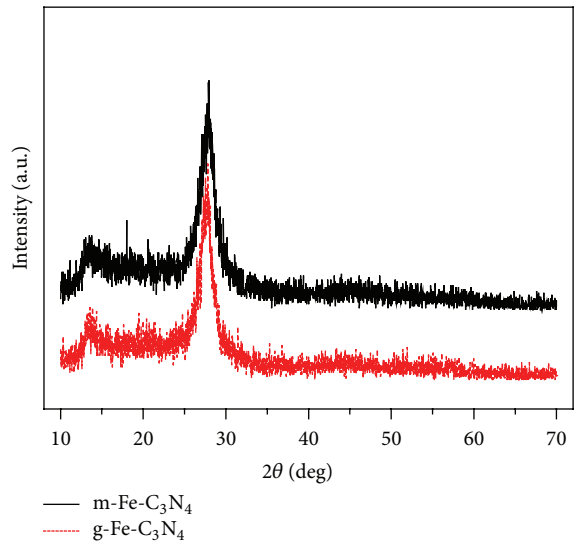

Figure 1: XRD patterns of the g-Fe-C_3N_4 and m-Fe-C_3N_4 samples.

2. Materials and Methods

2.1. Preparation of g-Fe-C_3N_4. Graphitic metal-containing carbon nitride compounds were synthesized according to the procedure reported previously [11]. Dicyandiamide was mixed with 0.12 g $FeCl_3$ in water (20 mL) under stirring, and then the mixed solution was heated at 100°C to remove water. The resulting powder was then heated at a rate of 2.3°C min^{-1} for about 4 h to reach a temperature of 550°C and then held at this temperature for an additional 4 h under flowing nitrogen gas. The sample was then cooled to room temperature and was denoted as g-Fe-C_3N_4.

2.2. Preparation of m-Fe-C_3N_4. A 5 wt% dispersion of 15 ± 5 nm SiO_2 particles in water (20 mL) was heated and stirred at 100°C with dicyandiamide (4 g, Aldrich) and $FeCl_3$ (0.12 g) added. The mixed solution was treated following the same procedures as mentioned above to obtain high-temperature power. The resulting power was then stirred in 200 mL of 4 mol/L NH_4HF_2 for 12 h, followed by filtration and washing with water. After that, the sample was cooled to room temperature and was denoted as m-Fe-C_3N_4.

3. Characterization

The morphology of the samples were observed using transmission electron microscopy (TEM, JEM-2011, JEOL Co., Japan). The nitrogen adsorption-desorption isotherms and Brunauer-Emmett-Teller (BET) surface areas were measured using a TriStar II 3020M instrument at 77 K. The crystal properties of the samples were identified by an 18 kW rotating anode X-ray diffractometer (MAP18AHF, MAC Sci. Co., Japan). The optical absorbance spectra of the samples were recorded using a UV-visible spectrophotometer (SolidSpec-3700, Shimadzu Co., Japan). The samples were ground with KBr power and pressed to form a uniform disk prior to FTIR analysis (Magna-IR 750, Nicolet Instrument Co., USA).

4. Photocatalytic Activity Measurement

Photocatalytic activities of samples for RhB degradation were evaluated with irradiation by a 500 W Xe lamp. In a Pyrex glass reactor, a total amount of 20 mg photocatalyst powder was dispersed in 40 mL of 5 mg L^{-1} aqueous solution of RhB. One mL suspension was sampled at fixed time intervals during the reaction. The suspension was centrifuged to remove the photocatalyst and then the concentration variation of RhB was examined by UV-vis spectrophotometer (UV-2450, Shimadzu Co., Japan).

5. Results and Discussion

XRD data obtained from both g-Fe-C_3N_4 and m-Fe-C_3N_4 are illustrated in Figure 1. All these patterns indicate a structural similarity between g-Fe-C_3N_4 and m-Fe-C_3N_4. There were two peaks in both samples. The strongest peak at 27.6, corresponding to an interlayer distance of 0.33 nm, could be indexed as the (002) peak of the stacking of the conjugated aromatic system [17]. However, XRD peak originated from iron species was not found in both samples. This indicates that mesoporous structure of metal-containing carbon nitride compounds did not disrupt the crystal structure of graphitic metal-containing carbon nitride compounds. Thus, it could be inferred that the iron species in m-Fe-C_3N_4 was chemically coordinated to the g-C_3N_4 host [12].

To get insight into the surface functionalities created by mesoporous structure, XPS measurements were performed. XPS survey scan spectra show C1s and N1s peaks at 288.1 eV and 398.7 eV in both the g-Fe-C_3N_4 and m-Fe-C_3N_4 samples (data not shown). The C1s binding energy shows mainly one carbon species, corresponding to a C–N–C coordination. In the N1s spectrum the main signal shows the existence of C–N–C groups [18]. The assignment of peaks in the C1s and N1s spectra of two samples was in good agreement with the literature report [12]. It could be seen that C–N bonds were

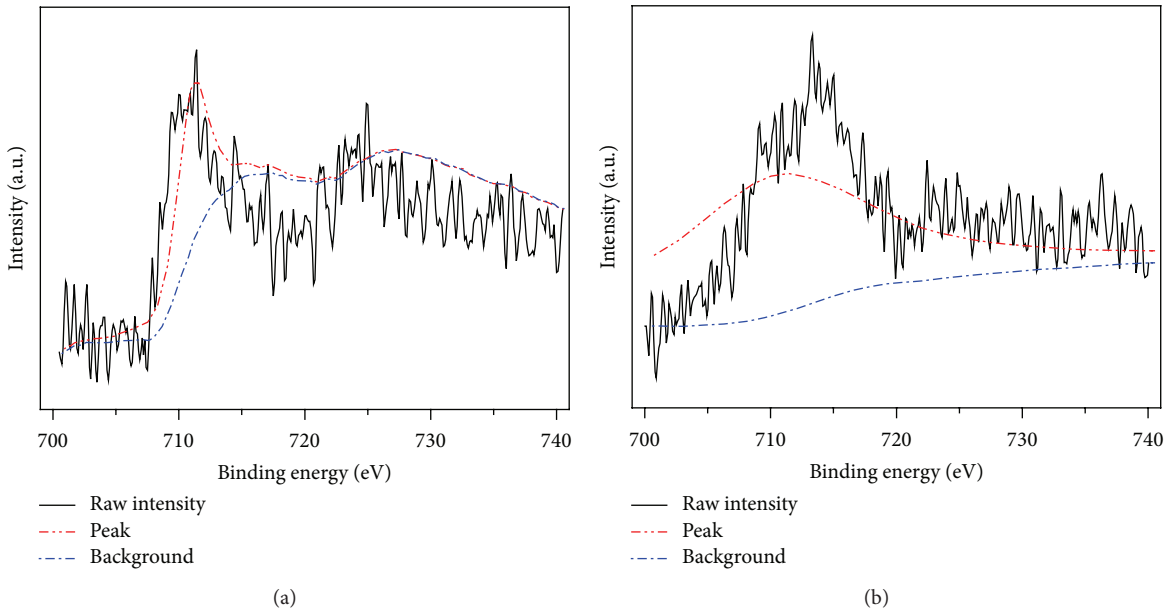

Figure 2: XPS spectra of Fe2p for g-Fe-C_3N_4 (a) and m-Fe-C_3N_4 (b).

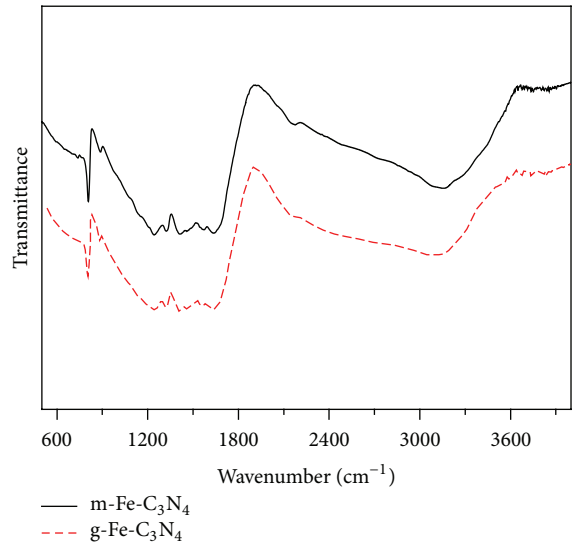

Figure 3: FTIR spectra of the g-Fe-C_3N_4 and m-Fe-C_3N_4 samples.

not broken by doping Fe and the formation of mesoporous structure, while the mesoporous structure strengthened C1s and N1s peaks. The high resolution Fe2p XPS spectra shown in Figure 2 are characterized by a broad peak in the range of 700–740 eV. The typical XPS spectrum of m-Fe-C_3N_4 revealed a Fe2p binding energy peak at 710.1 eV, which was lower than the value of 711.2 eV measured for g-Fe-C_3N_4. They all fell within the range of binding energy of Fe(III) state, and only a small amount of Cl could be detected. This result implies that Fe(III) is connected to C_3N_4 framework mainly through Fe–N bonds, while little was used for charge balance by Cl^- ions. Thus, Fe(III) in m-Fe-C_3N_4 might also be stabilized in the electron-rich C_3N_4 structure like g-Fe-C_3N_4.

Figure 3 shows the FTIR spectra of the g-Fe-C_3N_4 and m-Fe-C_3N_4 samples. They exhibit a peak at 808 cm^{-1} and several other major bands from 1200 to 1700 cm^{-1}. The two samples show stretching modes in the 1200–1700 cm^{-1} region, which were typical stretching modes of CN heterocycles originating from the extended C_3N_4 network [19], whereas the sharp band at about 808 cm^{-1} should be attributed to ring-sextant bending vibration characteristic of triazine or heptazine ring systems [20, 21]. The results indicate that both the samples were chemically coordinated to the C_3N_4 host and formed no metal nitrides or metal carbides.

Figure 4 shows TEM images of the g-Fe-C_3N_4 and m-Fe-C_3N_4 samples. These results indicate that the pore size

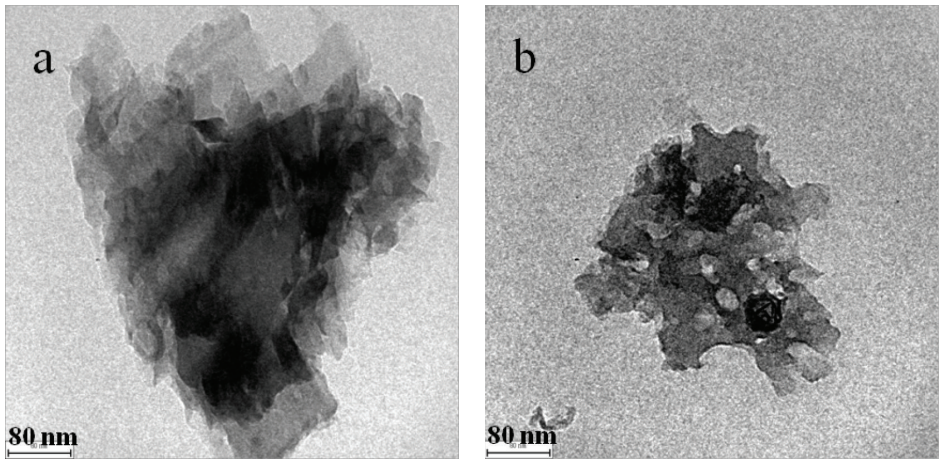

(a) (b)

Figure 4: TEM images of the g-Fe-C_3N_4 and m-Fe-C_3N_4 samples.

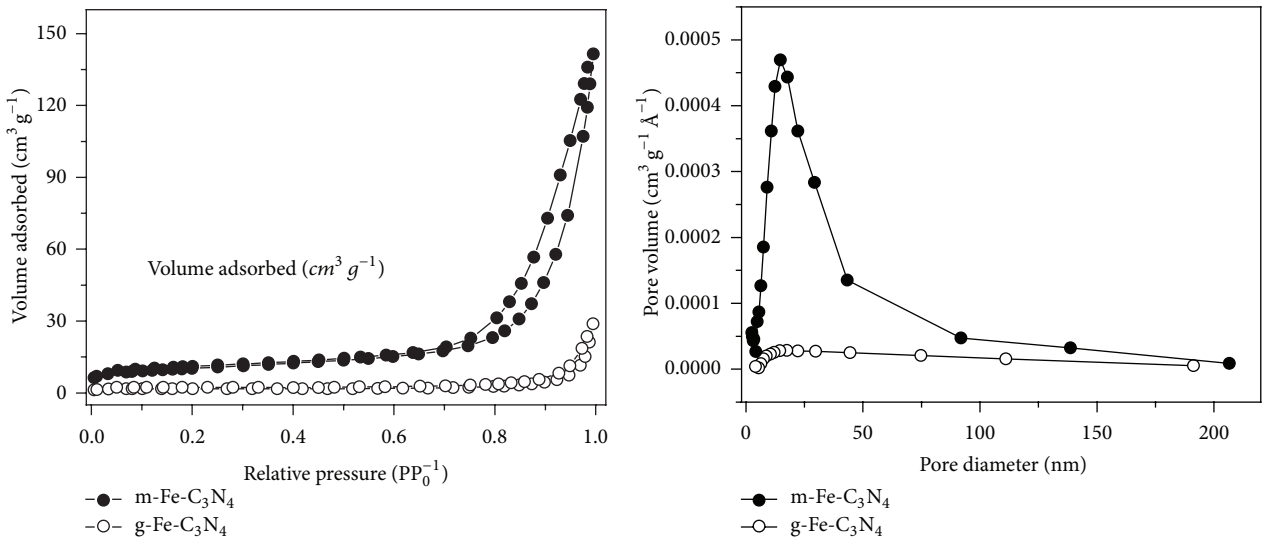

(a) (b)

Figure 5: N_2 adsorption-desorption isotherms (a) and Barret-Joyner-Halenda (BJH) pore size distribution plots (b) of g-Fe-C_3N_4 and m-Fe-C_3N_4 samples.

and connectivity of those powders exactly reflect the geometric properties of the original template [2]. The g-Fe-C_3N_4 shows a graphitic-like and two-dimensional layer structure (Figure 4(a)), which is similar to that of pure g-C_3N_4. The TEM image of m-Fe-C_3N_4 in Figure 4(b) shows disordered pore system of spherical pores with diameter of 15–20 nm, which is consistent with the size of SiO_2 template. Compared to g-Fe-C_3N_4, m-Fe-C_3N_4 exhibited a slightly less dense structure and a higher surface area.

Figure 5 shows nitrogen adsorption/desorption isotherms of the g-Fe-C_3N_4 and m-Fe-C_3N_4 samples. The isotherms of both samples exhibit type III behavior according to the IUPAC classification, indicating the existence of porous structures in the samples [22]. The BET surface area of the m-Fe-C_3N_4 sample (35.9 $m^2\,g^{-1}$) was much higher than that of m-Fe-C_3N_4 sample (5.7 $m^2\,g^{-1}$). The larger pore volume of m-Fe-C_3N_4 sample (0.17 $cm^3\,g^{-1}$) suggested that it was more porous compared with that of g-Fe-C_3N_4 sample (0.02 $cm^3\,g^{-1}$). An average pore diameter of 18.4 nm for m-Fe-C_3N_4 can be estimated from the BJH pore size distribution (Figure 5(b)). The pore size distribution of the two samples obtained from its absorption isotherm is consistent with the observed pore sizes from the TEM image. These results illustrate that m-Fe-C_3N_4 sample has been introduced with porous structure, which results in an increased surface area, enlarged pore volume, and narrow pore size distribution.

Figure 6 shows the optical absorbance spectra of the g-Fe-C_3N_4 and m-Fe-C_3N_4 samples. The absorption edge was at about 480 nm for g-Fe-C_3N_4 and 460 nm for m-Fe-C_3N_4, corresponding to the calculated band gap of ca. 2.58 and

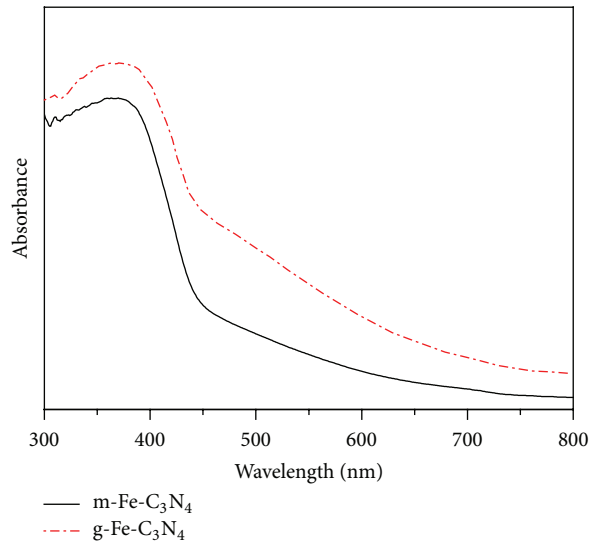

Figure 6: UV-vis absorption spectra of the g-Fe-C_3N_4 and m-Fe-C_3N_4 samples.

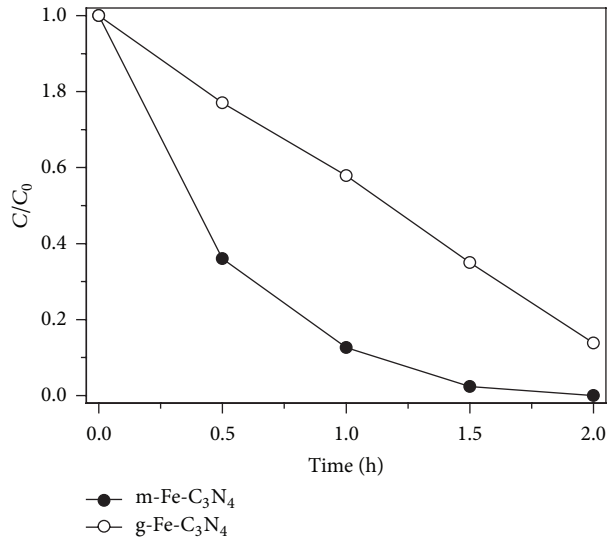

Figure 7: Comparison of the activities of g-Fe-C_3N_4 and m-Fe-C_3N_4 samples for RhB photocatalytic degradation.

2.70 eV, respectively. The comparison on the spectra of g-Fe-C_3N_4 and m-Fe-C_3N_4 samples indicates that the mesoporous structure of metal-containing carbon nitride compounds altered the electronic structure, and meantime the band gap was increased. Such structural change would lower the visible light response, though it might enhance the transport efficiencies of electrons and holes.

The photocatalytic performance of the resultant samples for RhB degradation under irradiation is shown in Figure 7. The results indicate that the mesoporous structure greatly influences the photocatalytic performance of g-Fe-C_3N_4 materials. The g-Fe-C_3N_4 showed a moderate photoreactivity toward organics degradation, which is consistent with the literature report [11]. Only ~42% of RhB was degraded in 60 min by g-Fe-C_3N_4 under irradiation, which is much lower than that of mesoporous samples. The m-Fe-C_3N_4 sample exhibits a higher photocatalytic activity, with nearly 88% and 98% of RhB degraded after 60 and 90 min irradiation, respectively. The m-Fe-C_3N_4 sample showed much higher efficiency in RhB degradation than g-Fe-C_3N_4 under irradiation. It is known that the photooxidation reactions of organic molecules can directly utilize the generated valence band holes or the main generated active species, $^{\bullet}OH$ radicals, from the reaction of holes with surface adsorbed water or hydroxyl groups [10]. The mesoporous structure is beneficial for promoting the mass transfer of reactants and products, enhancing the photocatalytic activity by facilitating access to the reactive sites on the surface photocatalyst. Generally, a larger surface area of photocatalysts is favorable for photocatalytic reaction by providing more possible reaction sites [23]. In addition, the unique electronic structure of m-Fe-C_3N_4 may also contribute considerably to the excellent photooxidation reactivity.

6. Conclusions

In summary, in situ Fe-doped mesoporous g-C_3N_4 was synthesized from a single precursor, dicyandiamide, by using SiO_2 nanoparticles as the template. The XRD results indicate that Fe is strongly coordinated with the g-C_3N_4 matrix and that the doping and mesoporous structure partly deteriorates its crystalline structure. The XPS analysis confirmed that Fe species was coordinated with the g-Fe-C_3N_4 and m-Fe-C_3N_4 framework through Fe–N bonds. The UV-visible absorption spectra reveal that the absorption edge of g-Fe-C_3N_4 was redshifted from 460 nm of the m-Fe-C_3N_4 sample to 480 nm together with a stronger light absorbance, implying that the formation of mesoporous structure changes the electronic properties of g-Fe-C_3N_4. The obtained Fe-doped mesoporous g-C_3N_4 shows much higher activity than the g-Fe-C_3N_4 for RhB degradation. This activity enhancement could be attributed to the increased surface area and unique mesoporous structure.

References

[1] Y. Wang, X. Wang, and M. Antonietti, "Polymeric graphitic carbon nitride as a heterogeneous organocatalyst: from photochemistry to multipurpose catalysis to sustainable chemistry," *Angewandte Chemie—International Edition*, vol. 51, no. 1, pp. 68–89, 2012.

[2] F. Goettmann, A. Fischer, M. Antonietti, and A. Thomas, "Chemical synthesis of mesoporous carbon nitrides using hard templates and their use as a metal-free catalyst for Friedel-Crafts reaction of benzene," *Angewandte Chemie—International Edition*, vol. 45, no. 27, pp. 4467–4471, 2006.

[3] X. Wang, K. Maeda, A. Thomas et al., "A metal-free polymeric photocatalyst for hydrogen production from water under visible light," *Nature Materials*, vol. 8, no. 1, pp. 76–80, 2009.

[4] P. Niu, G. Liu, and H. M. Cheng, "Nitrogen vacancy-promoted photocatalytic activity of graphitic carbon nitride," *The Journal of Physical Chemistry C*, vol. 116, no. 20, pp. 11013–11018, 2012.

[5] S. C. Yan, Z. S. Li, and Z. G. Zou, "Photodegradation performance of g-C_3N_4 fabricated by directly heating melamine," *Langmuir*, vol. 25, no. 17, pp. 10397–10401, 2009.

[6] M. Groenewolt and M. Antonietti, "Synthesis of g-C_3N_4 nanoparticles in mesoporous silica host matrices," *Advanced Materials*, vol. 17, no. 14, pp. 1789–1792, 2005.

[7] Y. Wang, H. Li, J. Yao, X. Wang, and M. Antonietti, "Synthesis of boron doped polymeric carbon nitride solids and their use as metal-free catalysts for aliphatic C-H bond oxidation," *Chemical Science*, vol. 2, no. 3, pp. 446–450, 2011.

[8] X. Wang, K. Maeda, X. Chen et al., "Polymer semiconductors for artificial photosynthesis: hydrogen evolution by mesoporous graphitic carbon nitride with visible light," *Journal of the American Chemical Society*, vol. 131, no. 5, pp. 1680–1681, 2009.

[9] Y. Wang, Y. Di, M. Antonietti, H. Li, X. Chen, and X. Wang, "Excellent visible-light photocatalysis of fluorinated polymeric carbon nitride solids," *Chemistry of Materials*, vol. 22, no. 18, pp. 5119–5121, 2010.

[10] G. Liu, P. Niu, C. Sun et al., "Unique electronic structure induced high photoreactivity of sulfur-doped graphitic C_3N_4," *Journal of the American Chemical Society*, vol. 132, no. 33, pp. 11642–11648, 2010.

[11] X. Wang, X. Chen, A. Thomas, X. Fu, and M. Antonietti, "Metal-containing carbon nitride compounds: a new functional organic-metal hybrid material," *Advanced Materials*, vol. 21, no. 16, pp. 1609–1612, 2009.

[12] Z. Ding, X. Chen, M. Antonietti, and X. Wang, "Synthesis of transition metal-modified carbon nitride polymers for selective hydrocarbon oxidation," *ChemSusChem*, vol. 4, no. 2, pp. 274–281, 2011.

[13] B. Yue, Q. Li, H. Iwai, T. Kako, and J. Ye, "Hydrogen production using zinc-doped carbon nitride catalyst irradiated with visible light," *Science and Technology of Advanced Materials*, vol. 12, no. 3, Article ID 034401, 7 pages, 2011.

[14] X. Chen, J. Zhang, X. Fu, M. Antonietti, and X. Wang, "Fe-g-C_3N_4-catalyzed oxidation of benzene to phenol using hydrogen peroxide and visible light," *Journal of the American Chemical Society*, vol. 131, no. 33, pp. 11658–11659, 2009.

[15] G. J. D. A. A. Soler-Illia, C. Sanchez, B. Lebeau, and J. Patarin, "Chemical strategies to design textured materials: from microporous and mesoporous oxides to nanonetworks and hierarchical structures," *Chemical Reviews*, vol. 102, no. 11, pp. 4093–4138, 2002.

[16] Y. Zhang, J. Liu, G. Wu, and W. Chen, "Porous graphitic carbon nitride synthesized via direct polymerization of urea for efficient sunlight-driven photocatalytic hydrogen production," *Nanoscale*, vol. 4, no. 17, pp. 5300–5303, 2012.

[17] F. Dong, L. Wu, Y. Sun, M. Fu, Z. Wu, and S. C. Lee, "Efficient synthesis of polymeric g-C_3N_4 layered materials as novel efficient visible light driven photocatalysts," *Journal of Materials Chemistry*, vol. 21, no. 39, pp. 15171–15174, 2011.

[18] A. Thomas, A. Fischer, F. Goettmann et al., "Graphitic carbon nitride materials: variation of structure and morphology and their use as metal-free catalysts," *Journal of Materials Chemistry*, vol. 18, no. 41, pp. 4893–4908, 2008.

[19] J. D. Hong, X. Y. Xia, Y. S. Wang, and R. Xu, "Mesoporous carbon nitride with in situ sulfur doping for enhanced photocatalytic hydrogen evolution from water under visible light," *Journal of Materials Chemistry*, vol. 22, pp. 15006–15012, 2012.

[20] B. V. Lotsch, M. Döblinger, J. Sehnert et al., "Unmasking melon by a complementary approach employing electron diffraction, solid-state NMR spectroscopy, and theoretical calculations-structural characterization of a carbon nitride polymer," *Chemistry—A European Journal*, vol. 13, no. 17, pp. 4969–4980, 2007.

[21] B. V. Lotsch and W. Schnick, "From triazines to heptazines: novel nonmetal tricyanomelaminates as precursors for graphitic carbon nitride materials," *Chemistry of Materials*, vol. 18, no. 7, pp. 1891–1900, 2006.

[22] G. Dong and L. Zhang, "Porous structure dependent photoreactivity of graphitic carbon nitride under visible light," *Journal of Materials Chemistry*, vol. 22, no. 3, pp. 1160–1166, 2012.

[23] E. Martínez-Ferrero, Y. Sakatani, C. Boissière et al., "Nanostructured titanium oxynitride porous thin films as efficient visible-active photocatalysts," *Advanced Functional Materials*, vol. 17, no. 16, pp. 3348–3354, 2007.